JGP Journal of General Physiology

ARTICLE

Myofilament Function 2022

RLC phosphorylation amplifies Ca^{2+} sensitivity of force in myocardium from cMyBP-C knockout mice

Kyrah L. Turner[1], Haley S. Morris[1], Peter O. Awinda[2], Daniel P. Fitzsimons[3], and Bertrand C.W. Tanner[2]

Hypertrophic cardiomyopathy (HCM) is the leading genetic cause of heart disease. The heart comprises several proteins that work together to properly facilitate force production and pump blood throughout the body. Cardiac myosin binding protein-C (cMyBP-C) is a thick-filament protein, and mutations in cMyBP-C are frequently linked with clinical cases of HCM. Within the sarcomere, the N-terminus of cMyBP-C likely interacts with the myosin regulatory light chain (RLC); RLC is a subunit of myosin located within the myosin neck region that modulates contractile dynamics via its phosphorylation state. Phosphorylation of RLC is thought to influence myosin head position along the thick-filament backbone, making it more favorable to bind the thin filament of actin and facilitate force production. However, little is known about how these two proteins interact. We tested the effects of RLC phosphorylation on Ca^{2+}-regulated contractility using biomechanical assays on skinned papillary muscle strips isolated from cMyBP-C KO mice and WT mice. RLC phosphorylation increased Ca^{2+} sensitivity of contraction (i.e., pCa_{50}) from 5.80 ± 0.02 to 5.95 ± 0.03 in WT strips, whereas RLC phosphorylation increased Ca^{2+} sensitivity of contraction from 5.86 ± 0.02 to 6.15 ± 0.03 in cMyBP-C KO strips. These data suggest that the effects of RLC phosphorylation on Ca^{2+} sensitivity of contraction are amplified when cMyBP-C is absent from the sarcomere. This implies that cMyBP-C and RLC act in concert to regulate contractility in healthy hearts, and mutations to these proteins that lead to HCM (or a loss of phosphorylation with disease progression) may disrupt important interactions between these thick-filament regulatory proteins.

Introduction

Hypertrophic cardiomyopathy (HCM) is a chronic heart disease characterized by decreased diastolic function and left ventricle hypertrophy. HCM affects 1 in every 200 people and is the most common cause of sudden cardiac death in athletes and young adults (Virani et al., 2020, Centers for Disease Control and Prevention, 2022). Clinical treatments for patients with HCM remain limited and focus on decreasing heart stress rather than treating the underlying genetic condition (Maron, 2010; Semsarian et al., 2015). The sarcomere, the fundamental structural unit underlying cardiac muscle contraction, contains thick filaments of myosin and thin filaments of actin. Along these filaments, actin–myosin crossbridge interactions generate the force and shortening to power cardiac contraction and blood circulation. It is well known that Ca^{2+} binding to the thin-filament regulatory proteins enable crossbridge binding. The mechanisms by which thick-filament regulatory proteins modulate crossbridge function remain less clear.

Genetic mutations in sarcomeric proteins can often be a preceding factor in HCM development (Marian, 2021). One of the most frequently mutated proteins associated with HCM clinical cases is cardiac myosin-binding protein-C (cMyBP-C). cMyBP-C is a thick-filament regulatory protein located in the c-zone of the cardiac sarcomere. cMyBP-C plays an important role in regulating contractility via interacting with the thick and thin filament with its N-terminal domain, and its C-terminus binds to the thick filament every three myosin crowns (Stelzer et al., 2006a; Stelzer et al., 2006b; Bhuiyan et al., 2016; Mun et al., 2014). Myosin regulatory light chain (RLC) is another thick-filament regulatory protein. RLC binds to the neck of the myosin-heavy chain, just between the catalytic "head" domain

[1]School of Molecular Biosciences & Neuroscience, Washington State University, Pullman, WA, USA; [2]Department of Integrative Physiology & Neuroscience, Washington State University, Pullman, WA, USA; [3]Department of Animal, Veterinary and Food Sciences, University of Idaho, Moscow, ID, USA.

Correspondence to Bertrand C.W. Tanner: bertrand.tanner@wsu.edu

This work is part of a special issue on Myofilament Function 2022.

and the coiled-coil "tail region." RLC undergoes posttranslational phosphorylation, which influences myosin head conformation and increases the probability of myosin binding to actin (Muthu et al., 2012; Toepfer et al., 2013; Breithaupt et al., 2019). Myosin heads that are positioned favorably to bind actin occupy the ON conformation, while folded myosin heads that cannot bind actin (i.e., the interacting heads motif) occupy the OFF conformation. Although the individual effects of these thick-filament regulatory proteins on contractile dynamics are starting to become more clear, it is unknown how cMyBP-C and RLC interact with each other to regulate cardiac function.

The cMyBP-C knockout mouse has been a useful transgenic model for characterizing the effects of cMyBP-C on cardiac contractility (Harris et al., 2002). Herein, we measured Ca^{2+}-activated force production and myosin crossbridge activity in permeabilized (skinned) myocardial strips as RLC phosphorylation was modulated in the presence or absence of cMyBP-C. We employed a series of biochemical and biophysical assays to further understanding of regulatory interactions between cMyBP-C and RLC, and how these interactions may affect contractile function in cMyBP-C knockout and WT mice.

Materials and methods

Animal models

All procedures were approved by the Institutional Animal Care and Use Committee at the University of Wisconsin-Madison and complied with the National Institutes of Health Guide for the Use and Care of Laboratory Animals. cMyBP-C KO animals were produced by the laboratory of Dr. Richard L. Moss as previously described (Harris et al., 2002). Following euthanasia, hearts were excised, cut along the long axis from base to apex, splayed open, flash-frozen in liquid nitrogen, and stored at the University of Wisconsin-Madison. Hearts were shipped overnight on dry ice to the University of Idaho and stored at −80°C until transported to Washington State University.

Cardiac histology

Hearts were thawed, dissected, submerged in embedding medium (O.C.T. Compound, 23-730-57; Thermo Fisher Scientific), and flash-frozen in isopentane at −140°C for 30 s and stored at −80°C until sectioned in a cryostat (model CM1860; Leica). Samples were sectioned at 10 µm thickness, placed on slides, and stored at −20°C until stained. Slides were fixed with 4% paraformaldehyde, stained with hematoxylin and eosin as previously described (Fenwick et al., 2019), and covered with glass coverslips. Images were acquired using LAS X imagine software, Leica DFC295 camera, and Nikon Eclipse E200 microscope at 0.4 numerical aperture and 200× total magnification. Image processing was performed using ImageJ.

Hydroxyproline assay

Cardiac fibrosis was assessed using a hydroxyproline colorimetric assay as previously described (Yuan et al., 2017). Briefly, 15 mg of left ventricle wall from each heart was placed in a glass vial containing 200 µl of 6 M HCl and incubated at 110°C overnight. In triplicate, 5 µl aliquots of the resulting solution were added to 80 µl of isopropanol, then mixed with 40 µl of a solution containing a 1:4 ratio of 7% w/v chloramine-T and acetate citrate buffer (0.695 M sodium acetate, 0.174 M citric acid, 0.435 M NaOH, and 38.5% isopropanol), and allowed to incubate at room temperature for 5 min. After incubation, 0.5 ml of the solution containing a 3:13 ratio of Ehrlich's solution and isopropanol was added to each sample and incubated at 55°C for 30 min. Samples were placed on ice to quench the reaction, and 200 µl of each sample was aliquoted to a 96-well plate. Absorbance was measured at 558 nm.

Solutions

Solution recipes were calculated and prepared as follows (Godt and Lindley, 1982), and all values are in mM where not otherwise specified. Relaxing solution: pCa 8.0 ($pCa = -\log_{10}[Ca^{2+}]$), 5 EGTA, 5 MgATP, 1 Mg^{2+}, 0.3 Pi, 35 phosphocreatine, 300 U/ml creatine kinase (CK), 200 ionic strength, 3% Dextran T-500 (w/v), and pH 7.0. Activating solution was the same as the relaxing solution, but adjusted to a free $[Ca^{2+}]$ of pCa 4.8. Dissecting solution: 50 BES, 30.83 K propionate, 10 Na azide, 20 EGTA, 6.29 $MgCl_2$, 6.09 ATP, 1 DTT, 20 BDM, 50 Leupeptin, 275 Pefabloc, and 1 E-64. Permeabilizing (skinning) solution: Dissecting solution with 1% Triton X-100 wt/vol and 50% glycerol wt/vol. Storage solution: Dissecting solution with 50% glycerol wt/vol. Alkaline phosphatase (AP) solution: relaxing solution with 170 U/ml AP (sc-3716; ChemCruz). Myosin light chain kinase (MLCK) solution: relaxing solution, but adjusted to pCa 6.25, 1.1 µM human skeletal MLCK, and 12 µM *Xenopus* calmodulin. MLCK sham solution: relaxing solution, but adjusted to pCa 6.25, 12 µM *Xenopus* calmodulin.

Muscle mechanics

Frozen hearts were placed in a vial with dissecting solution and left on ice for ∼10 min to thaw. Hearts were transferred onto a dissecting dish and papillary muscles were excised from the left ventricle. Papillary muscles were transferred to a dish containing skinning solution, trimmed, and skinned overnight at 4°C. Skinned papillary muscle strips were transferred to a storage solution, and if not used immediately for mechanics experiments, strips were stored at −20°C for up to 1 wk.

For all mechanics experiments, permeabilized left ventricular papillary muscles were trimmed to ∼180 µm in diameter and ∼700 µm in length. All strips were pretreated in AP solution for 10 min at room temperature prior to mounting. Aluminum T-clips were attached to the end of each strip and then mounted between a piezoelectric motor (P841.40; Physik Instrumente) and a strain gauge (AE801; Kronex), lowered into a 30 µl droplet of relaxing solution maintained at 28°C, and stretched to 2.2 µm sarcomere length measured by digital Fourier Transform (IonOptix Corp). Next, the strips were either incubated in MLCK solution or MLCK sham solution for 60 min, then relaxed to pCa 8.0, and the sarcomere length was checked again to confirm 2.2 µm. Following this, strips were Ca^{2+}-activated from pCa 8.0 to pCa 4.8. At least three strips from each heart underwent the same mechanics protocol at each condition, with the total number of strips and hearts listed in Table 1.

Table 1. **Characteristic values for steady-state isometric stress and three-parameter Hill fits to the Ca^{2+}-activated stress–pCa relationships**

	WT		cMyBP-C KO	
	AP	MLCK	AP	MLCK
F_{min} (kN m^{-2})	1.15 ± 0.10	1.37 ± 0.13	1.46 ± 0.12	1.55 ± 0.12
F_{abs} (kN m^{-2})	13.55 ± 0.55[a]	17.76 ± 0.85[b]	12.21 ± 0.51	12.49 ± 0.67
F_{dev} (kN m^{-2})	12.55 ± 0.53[a]	16.56 ± 0.85[b]	10.99 ± 0.47	11.15 ± 0.62
pCa_{50}	5.80 ± 0.02[a]	5.95 ± 0.03[b]	5.86 ± 0.02[a]	6.15 ± 0.03
n_H	6.32 ± 0.42	6.34 ± 0.68[b]	4.50 ± 0.38	4.48 ± 0.34
F_{max} (kN m^{-2})	13.06 ± 0.60[a]	16.50 ± 0.81[b]	11.14 ± 0.51	11.40 ± 0.67
n strips	21	19	18	22
n hearts	5		5	

F_{min}, absolute stress value at pCa 8.0; F_{abs}, absolute stress value at pCa 4.8; F_{dev}, Ca^{2+}-activated, developed stress ($T_{max} - T_{min}$); pCa_{50}, n_H, and F_{max} (= maximal stress) represent fit parameters to a three-parameter Hill equation for the F_{dev}-pCa relationship; *n* strips, total number of technical replicates (4–7 per heart); *n* hearts, number of biological replicates.
[a]P < 0.05 effect of MLCK treatment within the same genotype.
[b]P < 0.05 effect of genotype within same treatment type.

Sinusoidal length perturbations of 0.125% myocardial strip length (clip-to-clip) were applied at 44 discreet frequencies from 0.8 to 250 Hz to measure the complex modulus as a function of frequency (Kawai and Brandt, 1980; Mulieri et al., 2002; Palmer et al., 2007). The complex modulus represents viscoelastic myocardial stiffness, which arises from the change in stress divided by the change in muscle length that is in-phase (elastic modulus) and out-of-phase (viscous modulus) with the oscillatory length change at each frequency.

Characteristics of the elastic and viscous moduli responses over the measured frequency range provide a signature of crossbridge binding and cycling kinetics. Shifts in the elastic and viscous moduli are useful for assessing changes in the number of bound crossbridges between experimental conditions. In addition, shifts in the viscous modulus are useful for assessing changes in the work-producing and work-absorbing characteristics of the myocardium that arise from force-generating, cycling crossbridges. Frequencies producing negative viscous moduli represent regions of work-producing muscle function, with the "dip frequency" or frequency of the minimum viscous modulus describing force-generating events and the crossbridge recruitment rate (Awinda et al., 2020; Mulieri et al., 2002; Campbell et al., 2004). Frequencies producing positive viscous moduli represent regions of work-absorbing muscle function, with the "peak frequency" or frequency of the maximum viscous modulus describing crossbridge distortion events and crossbridge detachment rate (Awinda et al., 2020; Mulieri et al., 2002; Palmer et al., 2007, Palmer et al., 2011). These characteristic regions of minima and maxima in the viscous modulus versus frequency relationship were used to assess the effects of MLCK treatment on crossbridge kinetics under maximal Ca^{2+}-activated conditions. Given that viscous moduli were only measured at discrete frequencies, polynomials were fitted to regions of minimal viscous modulus (using 0.8–15-Hz data) and maximal viscous modulus (using 16–100-Hz data) using MATLAB (v9.11.0, The Mathworks) to create fitted curves at 0.05-Hz resolution. From these interpolated curves, we extracted the frequency of minimum viscous modulus and frequency of maximum viscous modulus.

Quantification of RLC phosphorylation in myocardial strips

After mechanical experiments were performed, permeabilized cardiac strips were homogenized, boiled for 5 min, chilled, and then stored at −80°C until gel electrophoresis. 12% acrylamide SDS-PAGE gels (BioRAD) were stained with Pro-Q diamond phosphostain and Sypro-Ruby total protein stain (Invitrogen). The intensity ratio of Pro-Q diamond to Sypro-Ruby was used to assess RLC phosphorylation levels. Average RLC phosphorylation was 10.3 ± 2.3% in AP-treated strips and 68.3 ± 2.4% in MLCK-treated strips, with no difference in phosphorylation levels between WT and cMyBP-C KO groups.

Statistical analysis

All statistical analyses were performed using SPSS (IBM Statistics). Unpaired Student's *t* test was performed to assess differences of hydroxyproline levels between genotypes. Nested linear mixed models incorporating one effect (treatment) were utilized to compare viscous and elastic moduli at each frequency for pCa 8.0 and 4.8 data, within each genotype. Nested linear mixed models incorporating two main effects (treatment and genotype) and their interaction were utilized for the stress–pCa fit parameters from three-parameter Hill fits, and for the minimum or maximum frequency parameters extracted from the polynomial curve that fits to the viscous moduli. Nested linear mixed model analyses link data from the same hearts, with hearts being a random effect, to optimize statistical power. Post-hoc analyses were performed using Fisher's least significant difference test, where P values < 0.05 were considered significant.

Results

cMyBP-C loss increases fibrosis and cellular disarray

Histological samples were stained with hematoxylin to visualize the cell nuclei and stained with eosin to visualize the cytoplasm of the cell. Representative images show increased cellular disorganization and fibrotic infiltration in the cMyBP-C KO myocardial samples (Fig. 1, A and B), as previously reported (Harris et al., 2002). Hydroxyproline assays were utilized to measure relative collagen content, or fibrosis levels, in myocardial tissue samples. Hydroxyproline is the most abundant amino acid in collagen, which represents the most abundant fibrotic component of the extracellular matrix. Hydroxyproline concentration was greater for cMyBP-C KO vs. WT samples, indicating increased fibrosis in cMyBP-C KO hearts (Fig. 1 C). Increased extracellular fibrosis due to the loss of cMyBP-C sarcomere contributes to myocardial remodeling that may lead to further contractile deficits.

Ca^{2+}-activated stress

Isometric stress increased as activating [Ca^{2+}] increased from pCa 8.0 to pCa 4.8, and these stress–pCa relationships were fit to a three-parameter Hill equation (Table 1). Maximal Ca^{2+}-activated stress (i.e., the increase in stress from the relaxed value at pCa 8.0) values were plotted against pCa for myocardial strips from WT and cMyBP-C KO mice. All strips were pretreated with AP, followed by a sham incubation or an MLCK incubation to phosphorylate RLC. AP treatment decreased the average phosphorylation to 10 ± 1% and MLCK treatment increased the average phosphorylation to 68 ± 3% (Fig. 2 C). There were no differences in the average RLC phosphorylation levels between genotypes. MLCK treatment increased Ca^{2+} sensitivity of contraction (as measured by pCa_{50}) and maximal Ca^{2+}-activated stress in the WT strips (Fig. 2 A), consistent with our prior findings using WT animals (Pulcastro et al., 2016). In the cMyBP-C KO strips, MLCK treatment increased Ca^{2+} sensitivity but not maximal Ca^{2+}-activated stress (Fig. 2 B and Fig. 3 B).

Normalizing stress–pCa curves of both genotypes to maximal stress within each condition helps show the differences in Ca^{2+} sensitivity between groups (Fig. 3 A). As introduced above, MLCK treatment increased Ca^{2+} sensitivity in both the WT and cMyBP-C KO strips, compared with their AP-treated controls (Fig. 3 C). However, pCa_{50} was most elevated in the MLCK-treated strips from cMyBP-C KO mice, indicating that MLCK treatment has an even greater effect on Ca^{2+} sensitivity when cMyBP-C is absent from the sarcomere. This suggests an interaction and/or coordination between RLC and cMyBP-C that regulates steady-state, isometric force production.

Viscoelasticity at relaxed and maximally activated conditions

Sinusoidal length–perturbation analysis was used to measure myocardial viscoelasticity and the effect of MLCK treatment on crossbridge cycling rates at both relaxed (pCa 8.0) and maximally activated conditions (pCa 4.8). Under relaxed conditions, there were no significant differences for the viscous or elastic moduli at any single frequency as a result of treatment or genotype (Fig. 4). For both WT and cMyBP-C KO strips at maximal Ca^{2+} activation, elastic moduli values were greater with MLCK treatment compared with AP-treated strips within each genotype (Fig. 5, A and B). Specifically, the elastic moduli values were larger at oscillatory frequencies >16 Hz for WT strips and frequencies >1.5 Hz for cMyBP-C KO strips. Similar to the elastic moduli differences, viscous moduli were greater for MLCK-treated strips than AP-treated strips at frequencies >65 Hz for

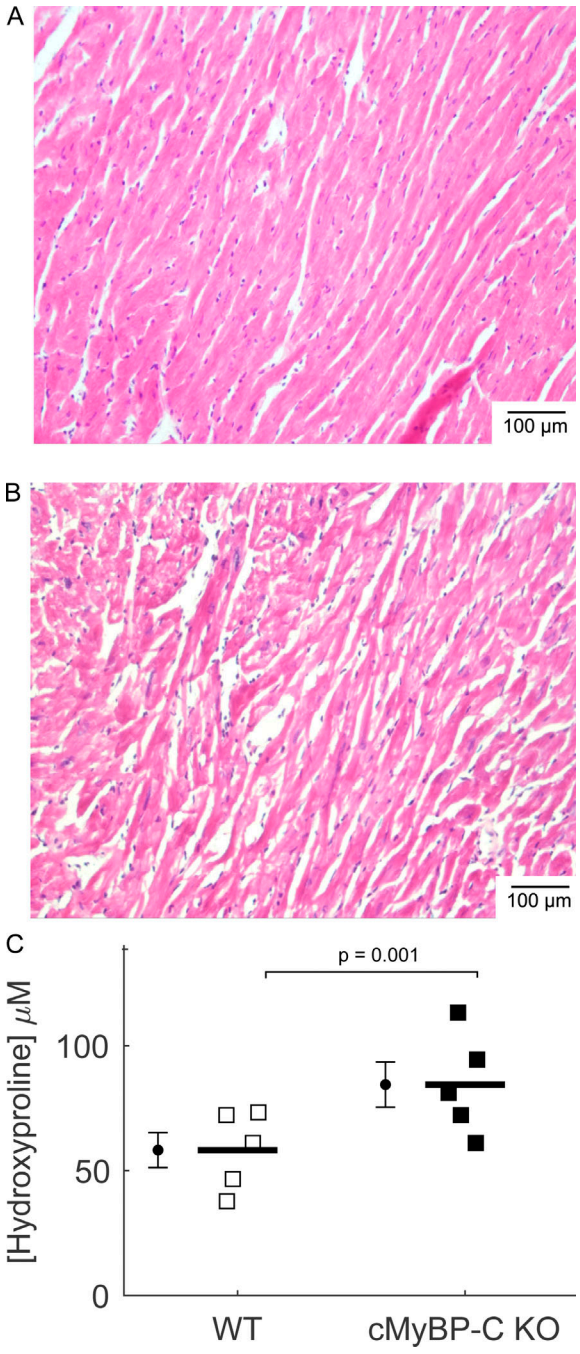

Figure 1. **cMyBP-C loss contributes to interstitial fibrosis. (A and B)** Myocardial sections from WT (A) and cMyBP-C KO (B) mice were stained with hematoxylin and eosin to characterize cellular organization and fibrosis. **(C)** Fibrosis levels were further quantified utilizing a hydroxyproline assay. Averages represent mean ± SEM, with individual data points shown for each heart. Individual data points represent the average of three technical replicates from five biological replicates per genotype.

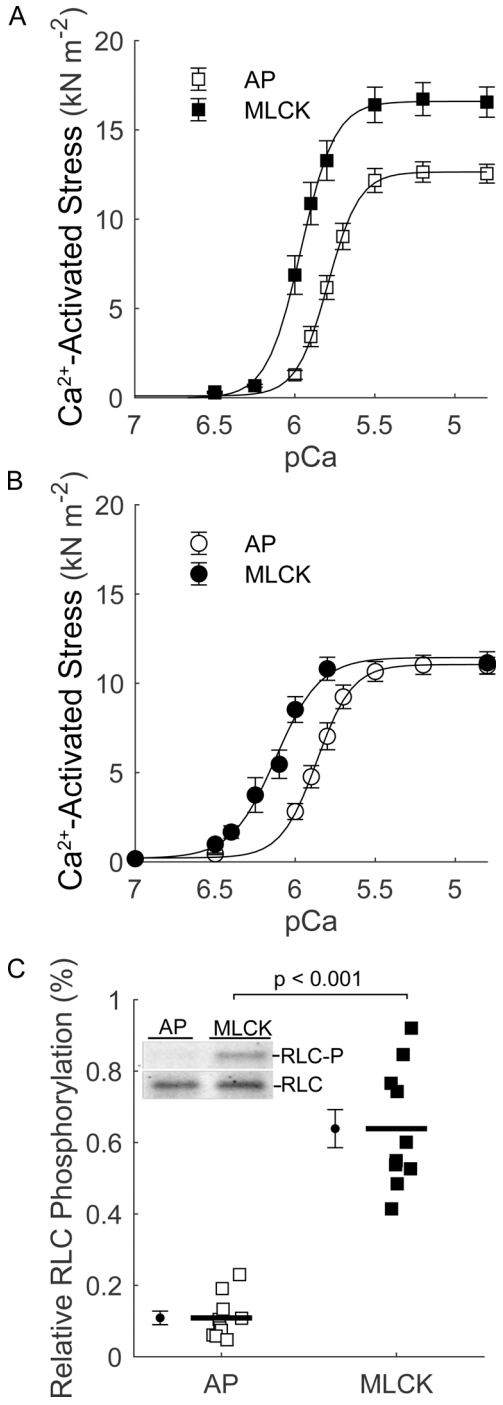

Figure 2. **RLC phosphorylation increases Ca^{2+} sensitivity of the stress–pCa relationships. (A and B)** Ca^{2+}-activated stress–pCa relationships for myocardial strips from WT (A) and cMyBP-C KO (B) mice with AP or MLCK treatment (mean ± SEM). Lines represent three-parameter Hill fits to the average stress–pCa data. **(C)** Relative RLC phosphorylation quantification by SYPRO Ruby and Pro-Q Diamond. Inset: Representative gel image for AP and MLCK treatment. The number of biological and technical replicates is listed in Table 1. Source data are available for this figure: SourceData F2.

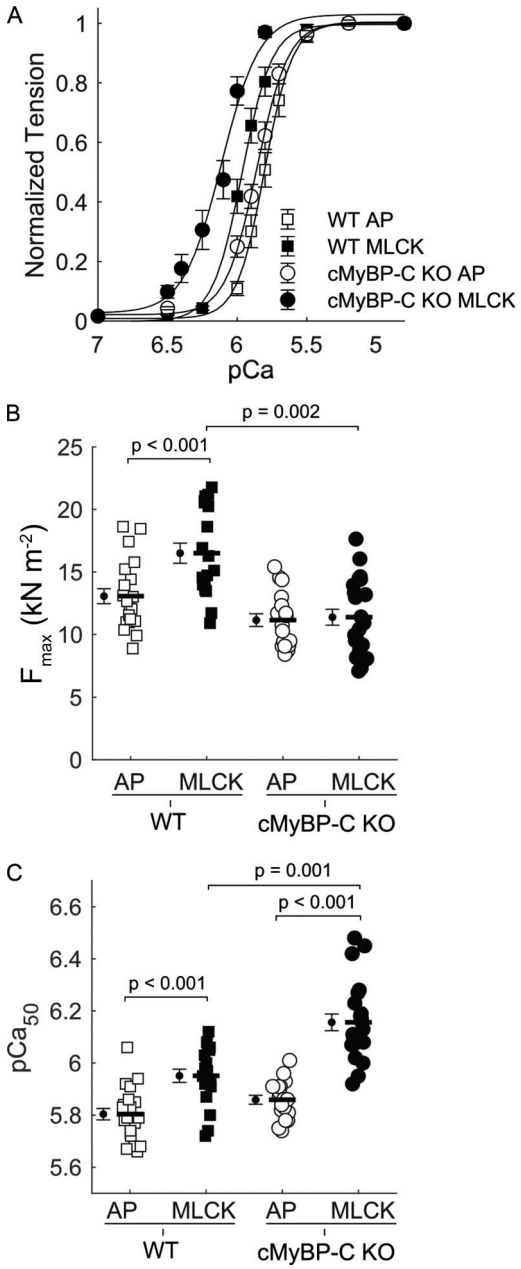

Figure 3. **RLC phosphorylation influences maximal force production and Ca^{2+} sensitivity. (A)** Normalized tension plotted against pCa shows the relative differences in Ca^{2+} sensitivity of contraction between all groups. **(B and C)** F_{max}, or maximal stress (fixed effects: genotype: P = 0.015; treatment: P = 0.001; genotype*treatment: P = 0.003; B), and pCa_{50} values from the three-parameter Hill fits (fixed effects: genotype: P = 0.015; treatment: P < 0.001; genotype*treatment: P = 0.005; C; Fig. 2 and Table 1). Averages represent mean ± SEM, with individual data points shown where applicable. The number of biological and technical replicates is listed in Table 1.

WT and between 20 and 25 Hz cMyBP-C KO (Fig. 5, C and D). In combination, this reflects more bound, cycling crossbridges or increased crossbridge stiffness in the MLCK-treated strips for both genotypes compared with AP-treated strips.

Frequency shifts in the viscoelastic system response result from changes in enzymatic crossbridge cycling kinetics during Ca^{2+}-activated conditions. The frequency of the minimum viscous modulus (i.e., the dip frequency for a single strip) was not different between WT and cMyBP-C strips, nor for MLCK-treated vs. AP-treated strips from cMyBP-C KO mice (Fig. 5 E). Albeit small, the dip frequency was slightly higher for MLCK-

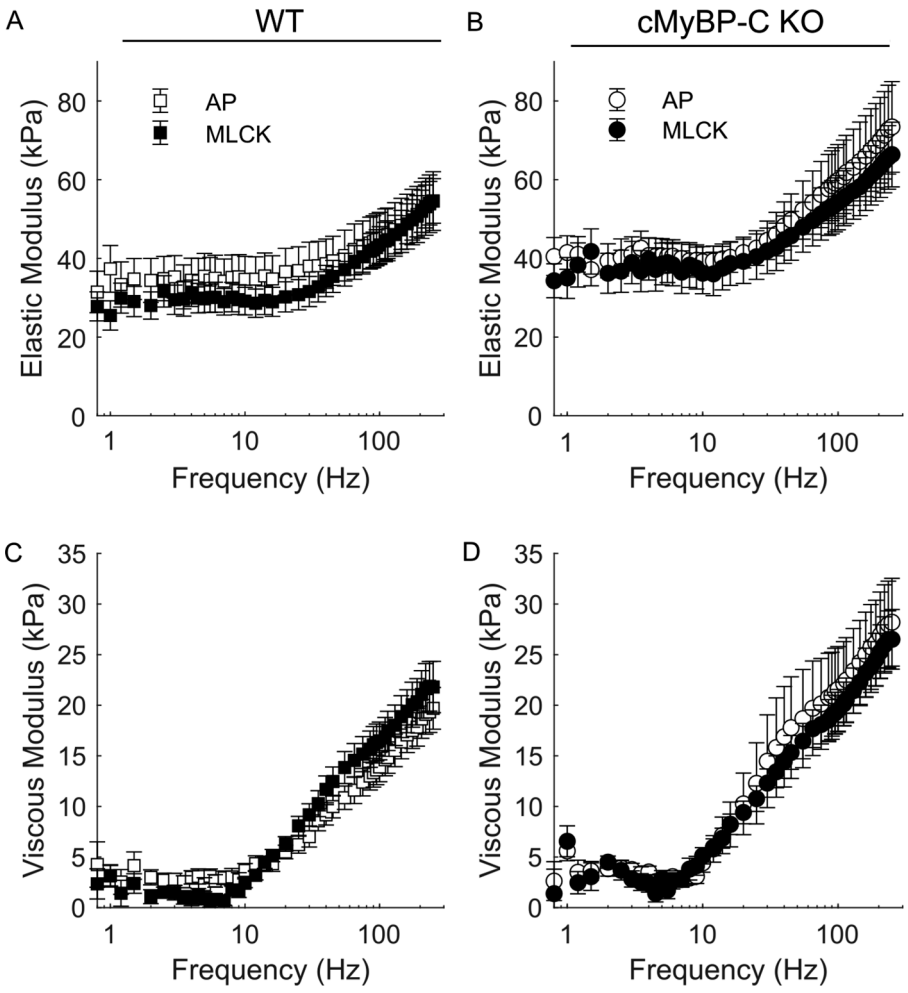

Figure 4. **RLC phosphorylation does not alter viscoelastic stiffness under relaxed conditions (pCa 8.0). (A–D)** Elastic moduli (A and B) and viscous moduli (C and D) values plotted against frequency for AP and MLCK treated strips from WT and cMyBP-C KO mice (mean ± SEM). The number of biological and technical replicates is listed in Table 1.

treated WT strips than AP-treated WT strips (Fig. 5, C and E), indicating a slightly faster crossbridge attachment rate for the MLCK-treated WT strips. We recognize that the slight increase in the dip frequency for MLCK-treated WT strips appears nearly equivalent to the average value of both treatment groups for cMyBP-C KO, although these latter two groups are not different from AP-treated WT strips (Fig. 5 E). A portion of this may follow from the different data distributions among all four groups and our nested linear mixed model analysis that clusters the technical replicates from each heart to elucidate biological differences more clearly than non-nested tests. With four to seven preparations of each treatment from each heart, the subtle statistical differences can be attributed to an increase in technical variation rather than a false biological difference. Nonetheless, any differences in crossbridge recruitment rate among the four groups are rather small.

Compared with WT strips, the frequency of the maximum viscous modulus (i.e., the peak frequency for a single strip) decreased for cMyBP-C KO strips, which indicates a slower crossbridge detachment rate in the absence of cMyBP-C (Fig. 5 F). Upon MLCK treatment, the peak frequency shifted toward a lower value for both genotypes (Fig. 5, C, D, and F), further suggesting that MLCK treatment slows crossbridge detachment (Pulcastro et al., 2016). Thus, the genotype and the treatment compound to confer the slowest detachment for the MLCK-treated cMyBP-C KO strips. In combination, these kinetics data suggest that removing cMyBP-C from the cardiac sarcomere may slow crossbridge detachment and the MLCK treatment slows the crossbridge detachment rate for WT and cMyBP-C strips.

Discussion

In this study, we performed muscle mechanics measurements to investigate the effect of RLC phosphorylation in permeabilized myocardial strips from WT and cMyBP-C KO mice. This enabled a relative assessment of the impact of RLC phosphorylation on the isometric stress–pCa relationship, myocardial viscoelasticity, and crossbridge cycling kinetics when cMyBP-C was either present or absent from the sarcomere. We found that cMyBP-C loss contributed to cellular modifications, such as increased fibrosis and cellular disorganization. RLC phosphorylation increased maximal force in the WT preparations, but not the cMyBP-C KO preparations. This difference could follow from increased fibrosis in the KO preparations, thereby compromising maximal force. RLC phosphorylation increased submaximal force production in strips from both genotypes, although RLC phosphorylation increased Ca^{2+} sensitivity of contraction more

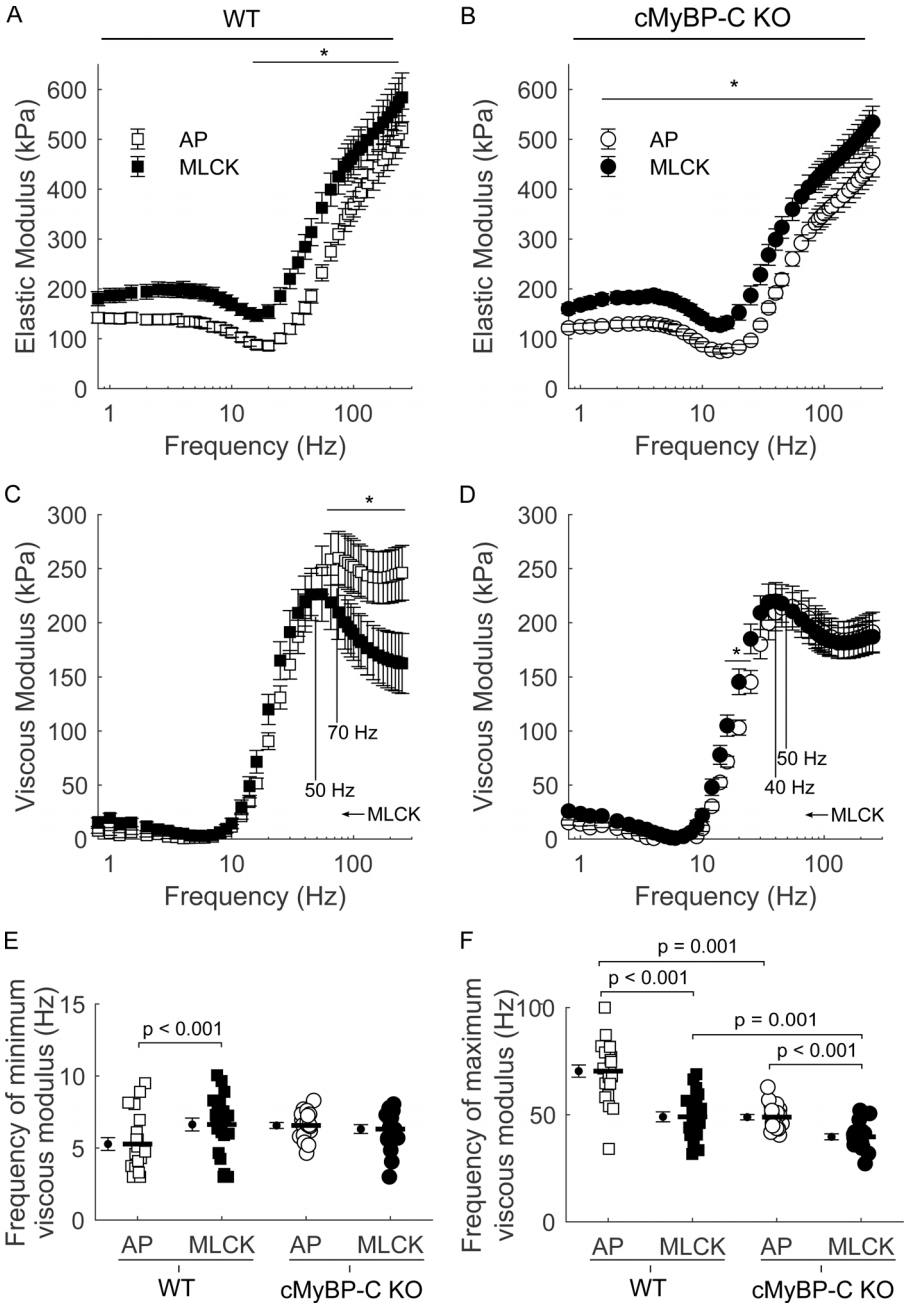

Figure 5. **RLC phosphorylation and cMyBP-C loss alter viscoelasticity and crossbridge kinetics under maximally activated conditions (pCa 4.8). (A–D)** Elastic moduli (A and B) and viscous moduli (C and D) values plotted against frequency for AP- and MLCK-treated strips from WT and cMyBP-C KO mice. **(E and F)** Frequency of the minimum viscous modulus represents a relative measure of crossbridge recruitment rate (fixed effects: genotype: P = 0.015; treatment: P = 0.001; genotype*treatment: P = 0.012; E) and frequency of the maximal viscous modulus represents a relative measure of the crossbridge detachment rate (fixed effects: genotype: P = 0.011; treatment: P = 0.001; genotype*treatment: P < 0.001; F). Averages represent mean ± SEM, with individual data points shown for each fiber where applicable. The number of biological and technical replicates is listed in Table 1.

in the cMyBP-C KO strips (by roughly twice as much). At maximal Ca^{2+} activation, RLC phosphorylation also increased myocardial stiffness (elastic modulus) for both genotypes, suggesting greater crossbridge binding or increased crossbridge stiffness with phosphorylated RLC. The increased stiffness was not obviously driven by differences in myofilament stiffness because myocardial viscoelasticity of relaxed strips (pCa 8.0) did not differ with genotype or RLC phosphorylation. RLC phosphorylation slowed crossbridge kinetics in WT and cMyBP-C KO strips, although crossbridge kinetics were slightly faster in WT strips. Thus, RLC phosphorylation may prolong the duration of myosin attachment to augment crossbridge contributions to thin-filament activation, and this mechanism was amplified when cMyBP-C was removed (or absent) from the sarcomere. Altogether these findings indicate that RLC and cMyBP-C likely interact with each other, acting in concert to regulate cardiac muscle contraction.

cMyBP-C phosphorylation throughout the cardiac sarcomere defines interactions between the N-terminus of cMyBP-C and the thin or thick filament. Native phosphorylation levels of cMyBP-C have been reported to exist at 50–60% (Previs et al., 2016; McNamara et al., 2019), and phosphorylation increases during β-adrenergic stimulation via the cAMP-dependent enzyme, protein kinase A (Sadayappan et al., 2009). We found that cMyBP-C phosphorylation levels in our WT papillary preparations were 42 ± 0.2% (SDS-PAGE with SYPRO Ruby and Pro-Q Diamond stains, data not shown) in our cardiac tissue samples from the WT mice. cMyBP-C phosphorylation levels did not

differ between AP and MLCK treatment, indicating that cMyBP-C phosphorylation is not affected by AP or MLCK. The 42% cMyBP-C phosphorylation level would be consistent with nearly half of the cMyBP-C being released from a thin-filament interaction (as occurs with cMyBP-C phosphorylation) and potentially interacting with the myosin S2 region. RLC also binds the S2 region of myosin, which allows for potential interactions between the N-terminus of cMyBP-C and RLC (Ponnam and Kampourakis, 2022; Pfuhl and Gautel, 2012). This may create an important "regulatory nexus" between cMyBP-C and RLC, given the developments of dual-filament regulation over the past decade (Zhang et al., 2017; Campbell et al., 2018; Kosta and Dauby, 2021; Awinda et al., 2020).

Phosphorylation of RLC is an essential mechanism to regulate cardiac contractility. RLC phosphorylation influences the conformation of the myosin heads, shifting them toward the ON or active state, closer to actin binding sites (Kampourakis and Irving, 2015; Sheikh et al., 2012). This structural shift increases the time acto-myosin crossbridges are bound, the force of contraction, Ca^{2+} sensitivity of contraction, and myocardial stiffness (Pulcastro et al., 2016; Khromov et al., 1998). In vitro motility assays using skeletal muscle myosin have shown that RLC phosphorylation slowed load-dependent crossbridge kinetics, thereby prompting speculation that RLC phosphorylation may increase myosin stiffness (Greenberg et al., 2009). Computational modeling of cardiac contractility showed that increased myosin stiffness with RLC phosphorylation could enhance twitch force and ventricular torsion throughout a heartbeat (Sheikh et al., 2012). While we did not directly measure myosin stiffness, we did measure viscoelastic myocardial stiffness under relaxed and activated conditions (Figs. 4 and 5). As strips are Ca^{2+} activated, the increases in viscoelastic myocardial stiffness are attributed to force-generating myosin crossbridges (Fig. 5). More specifically, the elastic modulus values show a clear increase under maximally activated conditions upon MLCK treatment for both genotypes. The range of frequencies where RLC phosphorylation significantly increased these moduli values (Fig. 5, A and B) was greater for the cMyBP-C KO strips, which supports the idea that RLC phosphorylation may have a greater relative impact on increases in crossbridge binding or crossbridge stiffness. Increases in crossbridge stiffness may alter nucleotide handling rates and "power-stroke" distances to augment crossbridge binding and force production with RLC phosphorylation, and to an even greater degree when cMyBP-C is absent from the sarcomere (Greenberg et al., 2009; Tanner et al., 2014; Wang et al., 2014).

Colson et al. (2010) also showed that RLC phosphorylation moved myosin heads away from thick filaments, closer to thin filaments, and that RLC phosphorylation simultaneously decreased thick-to-thin filament spacing. Eliminating cMyBP-C from the sarcomere did not affect thick-to-thin filament spacing (Colson et al., 2007). Therefore, it is possible that the RLC phosphorylation-dependent reduction in lattice spacing (~2%, at 2.15 µm sarcomere length; Colson et al., 2010) saturates or decreases at longer sarcomere lengths, such as the 2.2 µm sarcomere length utilized in this study. In addition, we utilized 3% Dextran T-500 to restore native thick-to-thin filament spacing that was disrupted during skinning (Kawai and Schulman, 1985; Kawai et al., 1993), which may overwhelm any subtle changes in lattice spacing due to RLC phosphorylation. To our knowledge, no previous studies have investigated the combined effects of increasing RLC phosphorylation and Dextran T-500 levels on lattice spacing per se. Nonetheless, it is likely that RLC-dependent decreases in thick-to-thin filament spacing and myosin head relocation toward the thin filament (away from the thick-filament backbone) could combine to increase the probability of crossbridge binding and decrease crossbridge detachment rate to augment force production.

We did not observe any clear increases in the crossbridge attachment rate (frequency of minimum viscous modulus; Fig. 5 E) with RLC phosphorylation or cMyBP-C loss, as previously reported (Stelzer et al., 2006a; Sweeney and Stull, 1990). Increases in crossbridge attachment rate have been associated with RLC phosphorylation repelling myosin heads away from the thick-filament backbone (Colson et al., 2010; Levine et al., 1998), which relocates them closer to their actin-binding sites along thin filaments. Alternatively, it is possible that RLC phosphorylation-dependent relocation of myosin heads could stabilize or promote strong crossbridge binding, thereby allowing crossbridges to remain bound longer and generate greater force (Tyska and Warshaw, 2002). The latter interpretation is consistent with the slower crossbridge detachment rates (frequency of maximum viscous modulus; Fig. 5 F) in the MLCK-treated strips from both genotypes.

Conflicting results have been reported regarding the role of cMyBP-C loss on crossbridge cycling kinetics, showing increases in crossbridge cycling rates (Harris et al., 2002; Korte et al., 2003; Stelzer et al., 2006b; Tong et al., 2008) and decreases in crossbridge cycling rates (Carrier et al., 2004; Pohlmann et al., 2007). A portion of the discrepancy may follow from the type of muscle preparation being studied. For example, de Lange et al. (2013) only observed increased crossbridge cycling kinetics in either single myocyte preparations derived from a cMyBP-C KO mouse model or human-derived engineered heart tissues with a cMyBP-C deletion. Neither of these preparations showed any hypertrophic remodeling and fibrosis. de Lang et al. (2013) did, however, observe decreased crossbridge cycling kinetics in multicellular preparations from cMyBP-C KO mice, in which hypertrophic remodeling and fibrosis were present. We also found slower detachment rates in our multicellular strips from cMyBP-C KO mice with demonstrated fibrosis (Fig. 1), consistent with prior studies using multicellular preparations with hypertrophic remodeling (Carrier et al., 2004; Pohlmann et al., 2007). It is well established that increased cardiac fibrosis results in relaxation deficits and dysregulated shortening velocities, likely due to increased myocardial stiffness (Burlew and Weber, 2002; Detterich, 2017; Moreo et al., 2009). Consequently, greater fibrosis may negatively impact muscle shortening and relaxation. The increased fibrosis observed in the multicellular preparations may alter how forces are transmitted throughout the myocardial strip and sarcomere, which may contribute to slowed crossbridge detachment rate (Fig. 5 F). A recent study by Hanft et al. (2021) showed slower maximal shortening velocity in permeabilized cardiomyocytes from

cMyBP-C KO at long sarcomere lengths (compared with controls), but similar maximal shortening velocities at short sarcomere length . Another study showed faster unloaded shortening velocity and faster time-to-peak twitch, but slower twitch relaxation and slower crossbridge kinetics in permeabilized myocardial strips from a cMyBP-C truncation mouse model (Palmer et al., 2004). Similarly, a recent study observed faster time-dependent unloaded shortening velocities in permeabilized myocardial strips from a cMyBP-C KO mouse model during submaximal activation (Giles et al., 2021). We speculate that the preparation type (myocyte vs. multicellular), permeabilization (skinned vs. intact), disease phenotype (pre-remodeling vs. hypertrophic remodeling and fibrosis), sarcomere length (short vs. long), and load (unloaded vs. loaded shortening) may all independently contribute to the differing contractile kinetics reported among these studies. Future investigation into cMyBP-C's regulatory role within the sarcomere will likely further elucidate its effects on each variable listed above in the context of contractile kinetics. RLC phosphorylation also led to decreased detachment rates, consistent with prior findings (Kampourakis and Irving, 2015; Pulcastro et al., 2016). In conjunction, both RLC phosphorylation and cMyBP-C loss contributed to slower detachment rates, and the combination of both effects may play a role in the increased Ca^{2+} sensitivity observed in cMyBP-C KO strips during RLC phosphorylation.

Altogether, our data show that (1) RLC phosphorylation enhances Ca^{2+} sensitivity of contraction in both genotypes, and (2) the effect of RLC phosphorylation on Ca^{2+} sensitivity is amplified when cMyBP-C is absent from the sarcomere. These findings suggest that RLC and cMyBP-C likely act in concert to contribute to contractility in healthy hearts. Prior studies have reported an interaction, or perhaps binding, between the C0 domain of cMyBP-C and RLC (Ratti et al., 2011; Bunch et al., 2018; Kampourakis and Irving, 2015; Pfuhl and Gautel, 2012; Ponnam et al., 2019), although the specific residues or number of RLC molecules with which cMyBP-C can interact are not well-defined. A plausible explanation for the amplified effects observed herein is the suppression of RLC activity by cMyBP-C's N-terminal binding to RLC. If the binding of the N-terminus of cMyBP-C and RLC does occur, this may directly alter RLC structure and/or function to mimic activity similar to decreased phosphorylation of RLC without altering the capacity for RLC to be phosphorylated (as demonstrated by the equal ability of WT and cMyBP-C KO preparations to be phosphorylated; Fig. 4). It may also be possible that cMyBP-C and RLC interact through a more indirect mechanisms that influence conformational transitions of either or both regulatory proteins, thereby influencing myocardial contractility. Future studies clarifying these interactions and how they may be disrupted with decreased RLC phosphorylation and/or common cMyBP-C mutations associated with heart disease may enlighten future therapeutic avenues to improve dysfunctional cardiac contraction.

Acknowledgments

Henk L. Granzier served as editor.

This work was supported by grants from the National Institutes of Health (R01 HL149164 to B.C.W. Tanner) and the American Heart Association (19TPA34860008 to B.C.W. Tanner).

The authors declare no competing financial interests.

Author contributions: K.L. Turner, D.P. Fitzsimons, and B.C.W. Tanner conceptualized the study. D.P. Fitzsimons procured and distributed the tissue samples. K.L. Turner, H.S. Morris, and P.O. Awinda performed the experiments. K.L. Turner, H.S. Morris, and P.O. Awinda analyzed and curated the data. K.L. Turner and B.C.W. Tanner wrote the original draft of the paper. K.L. Turner, D.P. Fitzsimons, and B.C.W. Tanner reviewed, edited, and revised additional versions of the manuscript, and all authors approved the final version submitted for review.

Submitted: 12 August 2022
Revised: 11 November 2022
Revised: 16 December 2022
Accepted: 18 January 2023

References

Awinda, P.O., Y. Bishaw, M. Watanabe, M.A. Guglin, K.S. Campbell, and B.C.W. Tanner. 2020. Effects of mavacamten on Ca^{2+} sensitivity of contraction as sarcomere length varied in human myocardium. *Br. J. Pharmacol.* 177:5609–5621. https://doi.org/10.1111/bph.15271

Bhuiyan, M.S., P. McLendon, J. James, H. Osinska, J. Gulick, B. Bhandary, J.N. Lorenz, and J. Robbins. 2016. In vivo definition of cardiac myosin-binding protein C's critical interactions with myosin. *Pflugers Arch.* 468:1685–1695. https://doi.org/10.1007/s00424-016-1873-y

Breithaupt, J.J., H.C. Pulcastro, P.O. Awinda, D.C. DeWitt, and B.C.W. Tanner. 2019. Regulatory light chain phosphorylation augments length-dependent contraction in PTU-treated rats. *J. Gen. Physiol.* 151:66–76. https://doi.org/10.1085/jgp.201812158

Bunch, T.A., V.C. Lepak, R.-S. Kanassatega, and B.A. Colson. 2018. N-terminal extension in cardiac myosin-binding protein C regulates myofilament binding. *J. Mol. Cell. Cardiol.* 125:140–148. https://doi.org/10.1016/j.yjmcc.2018.10.009

Burlew, B.S., and K.T. Weber. 2002. Cardiac fibrosis as a cause of diastolic dysfunction. *Herz.* 27:92–98. https://doi.org/10.1007/s00059-002-2354-y

Campbell, K.B., M. Chandra, R.D. Kirkpatrick, B.K. Slinker, and W.C. Hunter. 2004. Interpreting cardiac muscle force-length dynamics using a novel functional model. *Am. J. Physiol. Heart Circ. Physiol.* 286:H1535–H1545. https://doi.org/10.1152/ajpheart.01029.2003

Campbell, K.S., P.M.L. Janssen, and S.G. Campbell. 2018. Force-dependent recruitment from the myosin off state contributes to length-dependent activation. *Biophys. J.* 115:543–553. https://doi.org/10.1016/j.bpj.2018.07.006

Carrier, L., R. Knöll, N. Vignier, D.I. Keller, P. Bausero, B. Prudhon, R. Isnard, M.-L. Ambroisine, M. Fiszman, J. Ross Jr, et al. 2004. Asymmetric septal hypertrophy in heterozygous cMyBP-C null mice. *Cardiovasc. Res.* 63:293–304. https://doi.org/10.1016/j.cardiores.2004.04.009

Centers for Disease Control and Prevention. 2022. Heart disease facts. Available at: https://www.cdc.gov/heartdisease/facts.htm.

Colson, B.A., T. Bekyarova, D.P. Fitzsimons, T.C. Irving, and R.L. Moss. 2007. Radial displacement of myosin cross-bridges in mouse myocardium due to ablation of myosin binding protein-C. *J. Mol. Biol.* 367:36–41. https://doi.org/10.1016/j.jmb.2006.12.063

Colson, B.A., M.R. Locher, T. Bekyarova, J.R. Patel, D.P. Fitzsimons, T.C. Irving, and R.L. Moss. 2010. Differential roles of regulatory light chain and myosin binding protein-C phosphorylations in the modulation of cardiac force development. *J. Physiol.* 588:981–993. https://doi.org/10.1113/jphysiol.2009.183897

Detterich, J.A. 2017. Myocardial fibrosis: The heart of diastole? *Blood.* 130:104–105. https://doi.org/10.1182/blood-2017-05-786335

Fenwick, A.J., P.O. Awinda, J.A. Yarbrough-Jones, J.A. Eldridge, B.D. Rodgers, and B.C.W. Tanner. 2019. Demembranated skeletal and cardiac fibers

produce less force with altered cross-bridge kinetics in a mouse model for limb-girdle muscular dystrophy 2i. *Am. J. Physiol. Cell Physiol.* 317: C226–C234. https://doi.org/10.1152/ajpcell.00524.2018

Giles, J., D.P. Fitzsimons, J.R. Patel, C. Knudtsen, Z. Neuville, and R.L. Moss. 2021. cMyBP-C phosphorylation modulates the time-dependent slowing of unloaded shortening in murine skinned myocardium. *J. Gen. Physiol.* 153:e202012782. https://doi.org/10.1085/jgp.202012782

Godt, R.E., and B.D. Lindley. 1982. Influence of temperature upon contractile activation and isometric force production in mechanically skinned muscle fibers of the frog. *J. Gen. Physiol.* 80:279–297. https://doi.org/10.1085/jgp.80.2.279

Greenberg, M.J., T.R. Mealy, J.D. Watt, M. Jones, D. Szczesna-Cordary, and J.R. Moore. 2009. The molecular effects of skeletal muscle myosin regulatory light chain phosphorylation. *Am. J. Physiol. Regul. Integr. Comp. Physiol.* 297:R265–R274. https://doi.org/10.1152/ajpregu.00171.2009

Hanft, L.M., D.P. Fitzsimons, T.A. Hacker, R.L. Moss, and K.S. McDonald. 2021. Cardiac MyBP-C phosphorylation regulates the Frank–Starling relationship in murine hearts. *J. Gen. Physiol.* 153:202012770. https://doi.org/10.1085/jgp.202012770

Harris, S.P., C.R. Bartley, T.A. Hacker, K.S. McDonald, P.S. Douglas, M.L. Greaser, P.A. Powers, and R.L. Moss. 2002. Hypertrophic cardiomyopathy in cardiac myosin binding protein-C knockout mice. *Circ. Res.* 90:594–601. https://doi.org/10.1161/01.RES.0000012222.70819.64

Kampourakis, T., and M. Irving. 2015. Phosphorylation of myosin regulatory light chain controls myosin head conformation in cardiac muscle. *J. Mol. Cell. Cardiol.* 85:199–206. https://doi.org/10.1016/j.yjmcc.2015.06.002

Kawai, M., and P.W. Brandt. 1980. Sinusoidal analysis: A high resolution method for correlating biochemical reactions with physiological processes in activated skeletal muscles of rabbit, frog and crayfish. *J. Muscle Res. Cell Motil.* 1:279–303. https://doi.org/10.1007/BF00711932

Kawai, M., and M.I. Schulman. 1985. Crossbridge kinetics in chemically skinned rabbit psoas fibres when the actin-myosin lattice spacing is altered by dextran T-500. *J. Muscle Res. Cell Motil.* 6:313–332. https://doi.org/10.1007/BF00713172

Kawai, M., J.S. Wray, and Y. Zhao. 1993. The effect of lattice spacing change on cross-bridge kinetics in chemically skinned rabbit psoas muscle fibers. I. Proportionality between the lattice spacing and the fiber width. *Biophys. J.* 64:187–196. https://doi.org/10.1016/S0006-3495(93)81356-0

Khromov, A.S., A.V. Somlyo, and A.P. Somlyo. 1998. Thiophosphorylation of myosin light chain increases rigor stiffness of rabbit smooth muscle. *J. Physiol.* 512:345–350. https://doi.org/10.1111/j.1469-7793.1998.345be.x

Korte, F.S., K.S. McDonald, S.P. Harris, and R.L. Moss. 2003. Loaded shortening, power output, and rate of force redevelopment are increased with knockout of cardiac myosin binding protein-C. *Circ. Res.* 93: 752–758. https://doi.org/10.1161/01.RES.0000096363.85588.9A

Kosta, S., and P.C. Dauby. 2021. Frank-Starling mechanism, fluid responsiveness, and length-dependent activation: Unravelling the multiscale behaviors with an in silico analysis. *PLoS Comput. Biol.* 17:e1009469. https://doi.org/10.1371/journal.pcbi.1009469

de Lange, W.J., A.C. Grimes, L.F. Hegge, and J.C. Ralphe. 2013. Ablation of cardiac myosin-binding protein-C accelerates contractile kinetics in engineered cardiac tissue. *J. Gen. Physiol.* 141:73–84. https://doi.org/10.1085/jgp.201210837

Levine, R.J., Z. Yang, N.D. Epstein, L. Fananapazir, J.T. Stull, and H.L. Sweeney. 1998. Structural and functional responses of mammalian thick filaments to alterations in myosin regulatory light chains. *J. Struct. Biol.* 122:149–161. https://doi.org/10.1006/jsbi.1998.398

Marian, A.J. 2021. Molecular genetic basis of hypertrophic cardiomyopathy. *Circ. Res.* 128:1533–1553. https://doi.org/10.1161/CIRCRESAHA.121.318346

Maron, B.J. 2010. Contemporary insights and strategies for risk stratification and prevention of sudden death in hypertrophic cardiomyopathy. *Circulation.* 121:445–456. https://doi.org/10.1161/CIRCULATIONAHA.109.878579

McNamara, J.W., R.R. Singh, and S. Sadayappan. 2019. Cardiac myosin binding protein-C phosphorylation regulates the super-relaxed state of myosin. *Proc. Natl. Acad. Sci. USA.* 116:11731–11736. https://doi.org/10.1073/pnas.1821660116

Moreo, A., G. Ambrosio, B.D. Chiara, M. Pu, T. Tran, F. Mauri, and S.V. Raman. 2009. Influence of myocardial fibrosis on left ventricular diastolic function: Non-invasive assessment by CMR and ECHO. *Circ. Cardiovasc. Imaging.* 2:437–443. https://doi.org/10.1161/CIRCIMAGING.108.838367

Mulieri, L.A., W. Barnes, B.J. Leavitt, F.P. Ittleman, M.M. LeWinter, N.R. Alpert, and D.W. Maughan. 2002. Alterations of myocardial dynamic stiffness implicating abnormal crossbridge function in human mitral regurgitation heart failure. *Circ. Res.* 90:66–72. https://doi.org/10.1161/hh0102.103221

Mun, J.Y., M.J. Previs, H.Y. Yu, J. Gulick, L.S. Tobacman, S. Beck Previs, J. Robbins, D.M. Warshaw, and R. Craig. 2014. Myosin-binding protein C displaces tropomyosin to activate cardiac thin filaments and governs their speed by an independent mechanism. *Proc. Natl. Acad. Sci. USA.* 111: 2170–2175. https://doi.org/10.1073/pnas.1316001111

Muthu, P., K. Kazmierczak, M. Jones, and D. Szczesna-Cordary. 2012. The effect of myosin RLC phosphorylation in normal and cardiomyopathic mouse hearts. *J. Cell. Mol. Med.* 16:911–919. https://doi.org/10.1111/j.1582-4934.2011.01371.x

Palmer, B.M., D. Georgakopoulos, P.M. Janssen, Y. Wang, N.R. Alpert, D.F. Belardi, S.P. Harris, R.L. Moss, P.G. Burgon, C.E. Seidman, et al. 2004. Role of cardiac myosin binding protein C in sustaining left ventricular systolic stiffening. *Circ. Res.* 94:1249–1255. https://doi.org/10.1161/01.RES.0000126898.95550.31

Palmer, B.M., T. Suzuki, Y. Wang, W.D. Barnes, M.S. Miller, and D.W. Maughan. 2007. Two-state model of acto-myosin attachment-detachment predicts C-process of sinusoidal analysis. *Biophys. J.* 93: 760–769. https://doi.org/10.1529/biophysj.106.101626

Palmer, B.M., Y. Wang, and M.S. Miller. 2011. Distribution of myosin attachment times predicted from viscoelastic mechanics of striated muscle. *J. Biomed. Biotechnol.* 2011:592343. https://doi.org/10.1155/2011/592343

Pfuhl, M., and M. Gautel. 2012. Structure, interactions and function of the N-terminus of cardiac myosin binding protein C (MyBP-C): Who does what, with what, and to whom? *J. Muscle Res. Cell Motil.* 33:83–94. https://doi.org/10.1007/s10974-012-9291-z

Pohlmann, L., I. Kröger, N. Vignier, S. Schlossarek, E. Krämer, C. Coirault, K.R. Sultan, A. El-Armouche, S. Winegrad, T. Eschenhagen, and L. Carrier. 2007. Cardiac myosin-binding protein C is required for complete relaxation in intact myocytes. *Circ. Res.* 101:928–938. https://doi.org/10.1161/CIRCRESAHA.107.158774

Ponnam, S., and T. Kampourakis. 2022. Microscale thermophoresis suggests a new model of regulation of cardiac myosin function via interaction with cardiac myosin-binding protein C. *J. Biol. Chem.* 298:101485. https://doi.org/10.1016/j.jbc.2021.101485

Ponnam, S., I. Sevrieva, Y.-B. Sun, M. Irving, and T. Kampourakis. 2019. Site-specific phosphorylation of myosin binding protein-C coordinates thin and thick filament activation in cardiac muscle. *Proc. Natl. Acad. Sci. USA.* 116:15485–15494. https://doi.org/10.1073/pnas.1903033116

Previs, M.J., J.Y. Mun, A.J. Michalek, S.B. Previs, J. Gulick, J. Robbins, D.M. Warshaw, and R. Craig. 2016. Phosphorylation and calcium antagonistically tune myosin-binding protein C's structure and function. *Proc. Natl. Acad. Sci. USA.* 113:3239–3244. https://doi.org/10.1073/pnas.1522236113

Pulcastro, H.C., P.O. Awinda, J.J. Breithaupt, and B.C.W. Tanner. 2016. Effects of myosin light chain phosphorylation on length-dependent myosin kinetics in skinned rat myocardium. *Arch. Biochem. Biophys.* 601:56–68. https://doi.org/10.1016/j.abb.2015.12.014

Ratti, J., E. Rostkova, M. Gautel, and M. Pfuhl. 2011. Structure and interactions of myosin-binding protein C domain C0: Cardiac-specific regulation of myosin at its neck? *J. Biol. Chem.* 286:12650–12658. https://doi.org/10.1074/jbc.M110.156646

Sadayappan, S., J. Gulick, R. Klevitsky, J.N. Lorenz, M. Sargent, J.D. Molkentin, and J. Robbins. 2009. Cardiac myosin binding protein-C phosphorylation in a β-myosin heavy chain background. *Circulation.* 119: 1253–1262. https://doi.org/10.1161/CIRCULATIONAHA.108.798983

Semsarian, C., J. Ingles, M.S. Maron, and B.J. Maron. 2015. New perspectives on the prevalence of hypertrophic cardiomyopathy. *J. Am. Coll. Cardiol.* 65:1249–1254. https://doi.org/10.1016/j.jacc.2015.01.019

Sheikh, F., K. Ouyang, S.G. Campbell, R.C. Lyon, J. Chuang, D. Fitzsimons, J. Tangney, C.G. Hidalgo, C.S. Chung, H. Cheng, et al. 2012. Mouse and computational models link Mlc2v dephosphorylation to altered myosin kinetics in early cardiac disease. *J. Clin. Invest.* 122:1209–1221. https://doi.org/10.1172/JCI61134

Stelzer, J.E., S.B. Dunning, and R.L. Moss. 2006a. Ablation of cardiac myosin-binding protein-C accelerates stretch activation in murine skinned myocardium. *Circ. Res.* 98:1212–1218. https://doi.org/10.1161/01.RES.0000219863.94390.ce

Stelzer, J.E., D.P. Fitzsimons, and R.L. Moss. 2006b. Ablation of myosin-binding protein-C accelerates force development in mouse myocardium. *Biophys. J.* 90:4119–4127. https://doi.org/10.1529/biophysj.105.078147

Sweeney, H.L., and J.T. Stull. 1990. Alteration of cross-bridge kinetics by myosin light chain phosphorylation in rabbit skeletal muscle:

Implications for regulation of actin-myosin interaction. *Proc. Natl. Acad. Sci. USA*. 87:414–418. https://doi.org/10.1073/pnas.87.1.414

Tanner, B.C.W., Y. Wang, J. Robbins, and B.M. Palmer. 2014. Kinetics of cardiac myosin isoforms in mouse myocardium are affected differently by presence of myosin binding protein-C. *J. Muscle Res. Cell Motil.* 35: 267–278. https://doi.org/10.1007/s10974-014-9390-0

Toepfer, C., V. Caorsi, T. Kampourakis, M.B. Sikkel, T.G. West, M.-C. Leung, S.A. Al-Saud, K.T. MacLeod, A.R. Lyon, S.B. Marston, et al. 2013. Myosin regulatory light chain (RLC) phosphorylation change as a modulator of cardiac muscle contraction in disease. *J. Biol. Chem.* 288:13446–13454. https://doi.org/10.1074/jbc.M113.455444

Tong, C.W., J.E. Stelzer, M.L. Greaser, P.A. Powers, and R.L. Moss. 2008. Acceleration of crossbridge kinetics by protein kinase A phosphorylation of cardiac myosin binding protein C modulates cardiac function. *Circ. Res.* 103:974–982. https://doi.org/10.1161/CIRCRESAHA.108.177683

Tyska, M.J., and D.M. Warshaw. 2002. The myosin power stroke. *Cell Motil. Cytoskeleton*. 51:1–15. https://doi.org/10.1002/cm.10014

Virani, S.S., A. Alonso, E.J. Benjamin, M.S. Bittencourt, C.W. Callaway, A.P. Carson, A.M. Chamberlain, A.R. Chang, S. Cheng, F.N. Delling, et al. 2020. Heart disease and stroke statistics-2020 update: A report from the American heart association. *Circulation*. 141:e139–e596. https://doi.org/10.1161/CIR.0000000000000757

Wang, Y., K. Ajtai, and T.P. Burghardt. 2014. Ventricular myosin modifies in vitro step-size when phosphorylated. *J. Mol. Cell. Cardiol.* 72:231–237. https://doi.org/10.1016/j.yjmcc.2014.03.022

Yuan, C.-C., K. Kazmierczak, J. Liang, R. Kanashiro-Takeuchi, T.C. Irving, A.V. Gomes, Y. Wang, T.P. Burghardt, and D. Szczesna-Cordary. 2017. Hypercontractile mutant of ventricular myosin essential light chain leads to disruption of sarcomeric structure and function and results in restrictive cardiomyopathy in mice. *Cardiovasc. Res.* 113:1124–1136. https://doi.org/10.1093/cvr/cvx060

Zhang, X., T. Kampourakis, Z. Yan, I. Sevrieva, M. Irving, and Y.-B. Sun. 2017. Distinct contributions of the thin and thick filaments to length-dependent activation in heart muscle. *Elife*. 6:e24081. https://doi.org/10.7554/eLife.24081